CALCIUM SIGNALING

Copyright © 2022 The Authors, some rights reserved; exclusive licensee American Association for the Advancement of Science. No claim to original U.S. Government Works

Intravital calcium imaging in myeloid leukocytes identifies calcium frequency spectra as indicators of functional states

Fitsumbirhan T. Mehari[1,2], Meike Miller[1,2], Robert Pick[3], Almke Bader[2,3], Kami Pekayvaz[1,2,4], Matteo Napoli[3], Bernd Uhl[2,5], Christoph A. Reichel[2,5], Markus Sperandio[3], Barbara Walzog[2,3], Christian Schulz[1,2,4], Steffen Massberg[1,2,4], Konstantin Stark[1,2,4]*

The assessment of leukocyte activation in vivo is mainly based on surrogate parameters, such as cell shape changes and migration patterns. Consequently, additional parameters are required to dissect the complex spatiotemporal activation of leukocytes during inflammation. Here, we showed that intravital microscopy of myeloid leukocyte Ca^{2+} signals with Ca^{2+} reporter mouse strains combined with bioinformatic signal analysis provided a tool to assess their activation in vivo. We demonstrated by two-photon microscopy that tissue-resident macrophages reacted to sterile inflammation in the cremaster muscle with Ca^{2+} transients in a distinct spatiotemporal pattern. Moreover, through high-resolution, intravital spinning disk confocal microscopy, we identified the intracellular Ca^{2+} signaling patterns of neutrophils during the migration cascade in vivo. These patterns were modulated by the Ca^{2+} channel Orai1 and $G\alpha_i$-coupled GPCRs, whose effects were evident through analysis of the range of frequencies of the Ca^{2+} signal (frequency spectra), which provided insights into the complex patterns of leukocyte Ca^{2+} oscillations. Together, these findings establish Ca^{2+} frequency spectra as an additional dimension to assess leukocyte activation and migration during inflammation in vivo.

INTRODUCTION

The inflammatory responses to infections caused by pathogens and to sterile tissue damage involve the fine-tuned recruitment and activation of different leukocyte subpopulations. Monitoring their response to inflammatory stimuli in vivo is essential to understand this complex cellular activation pattern. However, leukocyte activation status in vivo is incompletely understood and mainly relies on surrogate parameters, such as migration patterns and cellular shape changes. Therefore, additional parameters of leukocyte activation are required to accurately assess the functional status of leukocytes in vivo.

Intracellular calcium (Ca^{2+}) signals are an ideal candidate for the real-time monitoring of leukocyte activity: Innate and adaptive immune cells depend on store-operated Ca^{2+} entry (SOCE) involving the Ca^{2+} sensor molecule stromal interaction molecule 1 (STIM1), which activates the calcium channel Orai1 to fulfill their roles in fighting infections. SOCE can be initiated by external factors through pathways including adhesion molecules, heterotrimeric GTP-binding protein (G protein)–coupled receptors (GPCRs) that couple to $G\alpha_i$ proteins, and mechanical stimuli. Defects in this process, for example, due to mutations in SOCE-regulating molecules, result in severe immune defects in humans (*1*–*3*). Whereas our knowledge of Ca^{2+} signaling and its functional importance is advanced in the case of adaptive immunity, it is less well explored in the context of innate immunity (*4*, *5*). Therefore, a detailed understanding of Ca^{2+} signals in vivo is necessary to obtain finer detail about the contributions of myeloid leukocytes to pathogen- and damage-associated injuries. For this purpose, we made use of power spectral density, which has been used to uncover diverse biologically relevant aspects of cellular activity in neuron firing activity (*6*), in comparing the Ca^{2+} signals of healthy and diseased neuronal network states (*7*) and in restoring cardiac autonomic control after ventricular hypertrophy (*8*).

In innate immune cells, Ca^{2+} signaling regulates their adhesion and migration, including rearrangements of the cytoskeleton, and activation of effector functions, such as phagocytosis, degranulation, and the production of reactive oxygen species (ROS) (*9*–*15*). In addition, a decrease in the rolling velocity of neutrophils in vivo correlates with an increase in intracellular free Ca^{2+} (*16*). On a molecular level, changes in intracellular Ca^{2+} concentration are mediated by SOCE, regulating Ca^{2+} influx; however, the contribution of Ca^{2+} influx to chemotaxis and the recruitment of neutrophils in mice remains unclear and is probably stimulus dependent (*17*–*19*). In this context, the mechanosensitive and store-operated cation channel of the transient receptor potential (TRP) family TRP channel 1 (TRPC1) has been identified as a modulator. The absence of TRPC1 leads to the decreased chemotaxis of neutrophils in vivo and in vitro (*20*). However, many aspects of intracellular signaling in neutrophils in vivo have been investigated with a zebrafish model (*21*). Through the in vivo imaging of phosphoinositide 3-kinase products, it has been shown that they differentially regulate neutrophil polarity and protrusion formation (*22*). Moreover, Ca^{2+} influx at the leading edge determined the directionality of neutrophil migration, as was shown by reversible and spatiotemporally controlled Ca^{2+} manipulation and imaging in live zebrafish (*23*). This analysis has been advanced by optogenetic approaches that enable the manipulation of Ca^{2+} concentration in leukocytes in vivo (*24*, *25*). Sudden increases followed by sudden decreases in cytosolic Ca^{2+} concentration (which are referred to as bursts) in neutrophils are not associated with the

[1]Medizinische Klinik und Poliklinik I, University Hospital, LMU Munich, 81377 Munich, Germany. [2]Walter Brendel Centre of Experimental Medicine, Faculty of Medicine, LMU Munich, 81377 Munich, Germany. [3]Institute for Cardiovascular Physiology and Pathophysiology, Walter Brendel Centre for Experimental Medicine, Biomedical Center (BMC), LMU Munich, 82152 Planegg, Germany. [4]German Center for Cardiovascular Research (DZHK), partner site Munich Heart Alliance, 80802 Munich, Germany. [5]Department of Otorhinolaryngology, University Hospital, LMU Munich, 81377, Munich, Germany.
*Corresponding author. Email: konstantin.stark@med.uni-muenchen.de

Downloaded from https://www.science.org at University Montpellier on September 11, 2023

formation of chemotactic protrusions in vitro but are stimulated by physical contact with a phagocytic target. This finding has led to the hypothesis that Ca^{2+} bursts control a mechanistic switch between distinct modes of cytoskeletal organization and dynamics (*26*).

The response of macrophages to inflammatory mediators also depends on Ca^{2+} but does not seem to solely rely on SOCE. Ca^{2+} signaling is involved in processes such as phagocytosis and cytokine production in macrophages (*27*, *28*). The Ca^{2+}-conducting ion channel transient receptor potential cation channel subfamily M member 7 (TRPM7) is necessary to induce inflammasome activation and cytokine release in response to bacterial lipopolysaccharide in macrophages (*29*, *30*). An increase in the abundance of the Ca^{2+}-permeable, nonselective cation channel TRPC6 in alveolar macrophages is caused by airway inflammation (*31*). Furthermore, the prototypical danger-associated molecular pattern (DAMP) high-mobility group box 1 (HMGB1) increases classical activation in macrophages (*32*). Because most tissue macrophages are immobile or show a slow, mesenchymal cell–like migration pattern (*33*) and do not show prominent changes in cell morphology in vivo, their response to inflammation has not yet been analyzed adequately by intravital microscopy. Using a zebrafish model, transgenic expression of fluorescent tumor necrosis factor–α has been applied for the in vivo assessment of macrophage polarization (*34*). In mice, sessile alveolar macrophages make use of synchronized Ca^{2+} waves for intercellular communication, exploiting the epithelium as a conducting system (*35*); however, the molecular mechanisms affecting Ca^{2+} flux in innate immune cells and how they reflect their functionality in vivo remain poorly understood.

Therefore, we performed intravital spinning disk confocal microscopy (SDCM) and two-photon microscopy, which provided high optical and temporal resolution, combined with transgenic Ca^{2+} reporter mouse strains to systematically assess Ca^{2+} signal patterns during the activation and migration of neutrophils and macrophages. This process enabled us to uncover the spatiotemporal-dependent activation of macrophages and neutrophils in the context of sterile inflammation in vivo. In neutrophils, we uncovered distinct Ca^{2+} signal patterns through the analysis of frequency spectra during the recruitment cascade, as well as the roles of Orai1 and $G\alpha_i$-coupled GPCRs in regulating Ca^{2+} dynamics and neutrophil migration in vivo.

RESULTS

Intravital Ca^{2+} imaging in myeloid leukocytes with subcellular resolution using a transgenic Ca^{2+} reporter mouse strain

To systematically detect Ca^{2+} signals in myeloid leukocytes in vivo, we adopted a Ca^{2+} reporter mouse strain previously described for use in neurons. In these mice, intracellular Ca^{2+} transients can be examined through the Ca^{2+} indicator GCaMP5G, which generates a Ca^{2+} binding–dependent green fluorescent protein (GFP) signal with a temporal resolution in the range of milliseconds (*36*). First, we used the ear model in *CX3CR1^{Cre}-GcaMP5G-IRES-tdTomato$^{fl/fl}$* mice for labeling and Ca^{2+} imaging in macrophages in combination with the slower but deeper-penetrating (as compared to SDCM) intravital two-photon microscope. This enabled long-term imaging with minimal bleaching and enabled us to capture Ca^{2+} oscillations in tissue macrophages. In response to a laser-induced injury, macrophages showed a complex spectrum with highly variable frequency and amplitude of Ca^{2+} signal (Fig. 1A). We also observed in *LysM^{Cre}-GcaMP5G-IRES-tdTomato$^{fl/fl}$* mice during neutrophil rolling and adhesion using SDCM in the cremaster muscle model that the constitutive tdTomato signal (a cytosolic red fluorescent protein that labels LysM$^+$ cells) remained relatively unchanged as opposed to the highly dynamic Ca^{2+}-GFP signal, which was lined with peaks and troughs (Fig. 1, B and C, and movie S1). The validity of this mouse model was further confirmed by in vitro imaging of HMGB1-treated peritoneal macrophages, which also showed Ca^{2+} oscillations in response to this inflammatory stimulus (Fig. 1, D and E, and movie S2). Therefore, the *GcaMP5G-IRES-tdTomato$^{fl/fl}$* mouse model together with Cre reporter strains for myeloid leukocytes enables an in vivo assessment of Ca^{2+} signals with high temporal and spatial resolution.

Detrending and filtering of Ca^{2+} signals are required to acquire analysis parameters

Ca^{2+} signals from in vivo settings are inherently prone to systematic shifts and noise. To uncover the underlying signal patterns, a detrending process must be performed to ensure that any systematic drifts, for example, tissue drift and bleaching, have no effects on further analyses. Inherent peaks in the signal originating from Ca^{2+} bursts are not affected by the detrending process. Detrending accentuated the peaks and centered the mean of the signal to zero (Fig. 2A). Detrended signals were then smoothened through the MATLAB built-in Savitzky-Golay filter (SGolayFilt) function. SGolayFilt was effective in smoothening the Ca^{2+} signals (Fig. 2A). A strict ruleset on how to select meaningful peaks and troughs is crucial to prevent noise from being detected as Ca^{2+} peaks and to compare across the same detrending and filtering settings. Hence, a ruleset consisting of SGolayFilt and minimum peak prominence (MPP; Materials and Methods and Eq. 5), a function that seeks to eliminate unnecessarily small peaks and troughs smaller than a percentage of the highest peak amplitude (HPA; Eq. 4), was put in place. The HPA is defined as the difference between the highest peak and the lowest trough. Therefore, a smaller MPP value means a highly unselective ruleset that leads to unselective quantitative results (Fig. 2A). A point is considered a peak if at least on either of its sides there is a reduction of $>0.1 \times p$ to the previous or next sample point (Fig. 2A), where p is a percentage value of the difference between the maximum and the minimum of the normalized intensity.

Frequency in Ca^{2+} oscillations is defined as the number of peaks in a specified amount of time, but this approach suffers from lack of information because Ca^{2+} signals are highly irregular. To overcome this, we converted the Ca^{2+} signal from the time domain to the frequency domain through Fourier transformation. The result is a display of all of the frequencies present in the signal arranged by their respective power, which is called the power spectrum density (PSD) and provides a detailed picture of the frequency ranges at which the Ca^{2+} signals appeared. This transformation enabled the identification of the frequency spectrum and the most dominant frequencies (Fig. 2, B and C). In conclusion, a series of normalization, detrending, filtering, and Fourier transformation steps of the Ca^{2+} signal is required to characterize it.

Spatiotemporal changes in Ca^{2+} signals in macrophages and neutrophils upon tissue injury

Tissue-resident macrophages are considered to be the first responders to sterile inflammation, but the in vivo evidence for this hypothesis is limited. When we assessed tissue-resident macrophages in *CX3CR1-GFP* mice by intravital two-photon microscopy after laser injury in the skin, we could not detect any changes in cellular morphology, and the cells remained immotile for the first 2 hours (fig. S1). To

Downloaded from https://www.science.org at University Montpellier on September 11, 2023

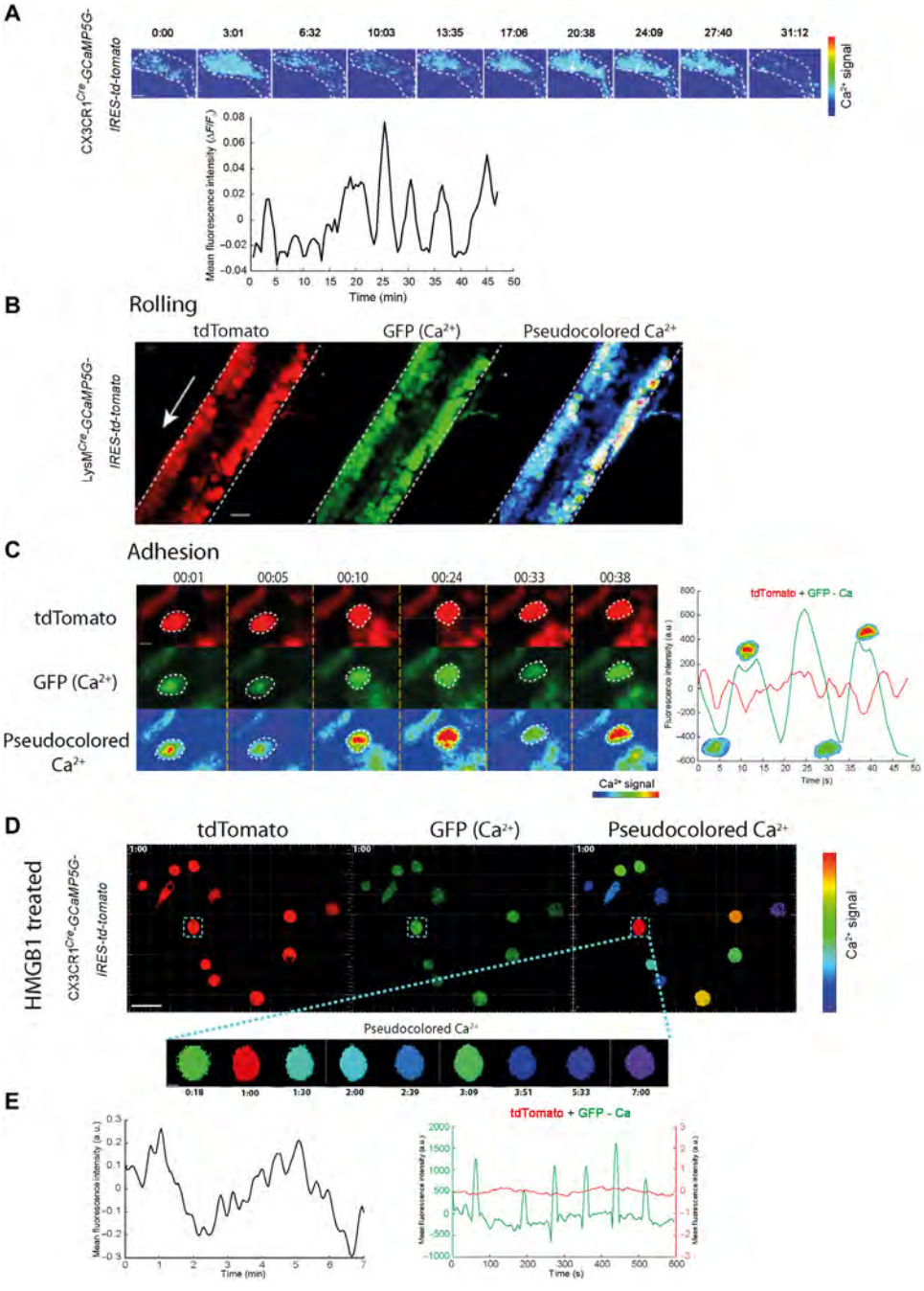

Fig. 1. Ca^{2+} signal reproducibility in vivo and in vitro. (**A**) Top: Representative time-lapse images of a tissue-resident macrophage showing intermittent surges in Ca^{2+} signal (pseudocolored bar) after laser injury. Scale bar, 5 μm. Time is indicated in min:s. Bottom: Mean fluorescence intensity time plot of the corresponding macrophage. (**B**) Time projection of neutrophils rolling in the vasculature (direction of flow indicated by the arrow) depicted in constitutive tdTomato signal and Ca^{2+} signal in GFP and pseudocolored modes. Scale bar, 20 μm. (**C**) Left: Time-lapse images of the constitutive tdTomato signal and Ca^{2+} signal in GFP and pseudocolored modes from a representative adherent neutrophil. Scale bar, 5 μm. Time is indicated in min:s. Right: Mean fluorescence intensity time plot tracings of the Ca^{2+} signal (green) and constitutive tdTomato signal (red) of the corresponding cell. a.u., arbitrary units. (**D**) Constitutive tdTomato signal and Ca^{2+} signal in GFP and pseudocolored modes of peritoneal macrophages in vitro after treatment with HMGB1. Scale bar, 30 μm. Bottom: Magnified time-lapse images of the Ca^{2+} signal in pseudocolored mode in a single cell. Scale bar, 5 μm. Time is indicated in min:s. (**E**) Left: Mean fluorescence intensity time plot tracings of the normalized Ca^{2+} signal of the cell shown in (D). Right: Mean fluorescence intensity time plot tracings of the Ca^{2+} signal (green) and the constitutive tdTomato signal (red) of the same cell. Images are representative of three experiments.

overcome these limitations of intravital microscopy, we tested whether and how changes in the intracellular Ca^{2+} signal could serve as a marker of macrophage activation in experiments with *CX3CR1*^{Cre}*-GCaMP5G-IRES-tdTomato*$^{fl/fl}$ mice. During basal conditions, $CX3CR1^+$ cells had very low amounts of Ca^{2+} signal (Fig. 3A and movie S3). This was substantially changed after the induction of sterile inflammation by a laser injury, and most of the $CX3CR1^+$ macrophages then exhibited frequent, short Ca^{2+} transients (<2 min), whereas some cells exhibited long transients (>2 min) of greater amplitude and more diverse frequency values than those of the oscillations seen in resting cells (Fig. 3, B and C). Because the cytokine interleukin-1β (IL-1β) is involved in the immune response to sterile inflammation, we stimulated peritoneal macrophages in vitro with increasing concentrations of IL-1β. A dose-dependent change in their normalized Ca^{2+} intensity and amplitude was observed up to a concentration of 1 ng/ml but not in terms of dominant frequency (defined as the frequency with the highest power; Fig. 3D). Analysis of the PSD spectra analogously showed substantially distinct signatures at the three different concentrations of IL-1β, mainly regarding the overall power but less so regarding the frequency spectrum (Fig. 3E). In summary, sterile inflammation by focal necrosis resulted in the activation of tissue-resident macrophages as evidenced by increases in Ca^{2+} intensity, amplitude, and frequency (Fig. 3F).

Because we hypothesized that focal necrosis generates gradients of DAMPs, chemokines, and lipid mediators depending on the distance from the site of necrosis, we investigated whether the activation status and Ca^{2+} signals of tissue macrophages were also similarly influenced (*37*). We found that $CX3CR1^+$ cells in close proximity to the site of necrosis were activated earlier than those farther from the site and that they showed increased activity as indicated by overall Ca^{2+} signal intensity, number of Ca^{2+} transients, and the percentage of cells with transients (Fig. 4, A and B, and movie S4). Moreover, we found that $CX3CR1^+$ cells nearer the necrosis site were activated earlier than neutrophils were recruited from the blood stream

Downloaded from https://www.science.org at University Montpellier on September 11, 2023

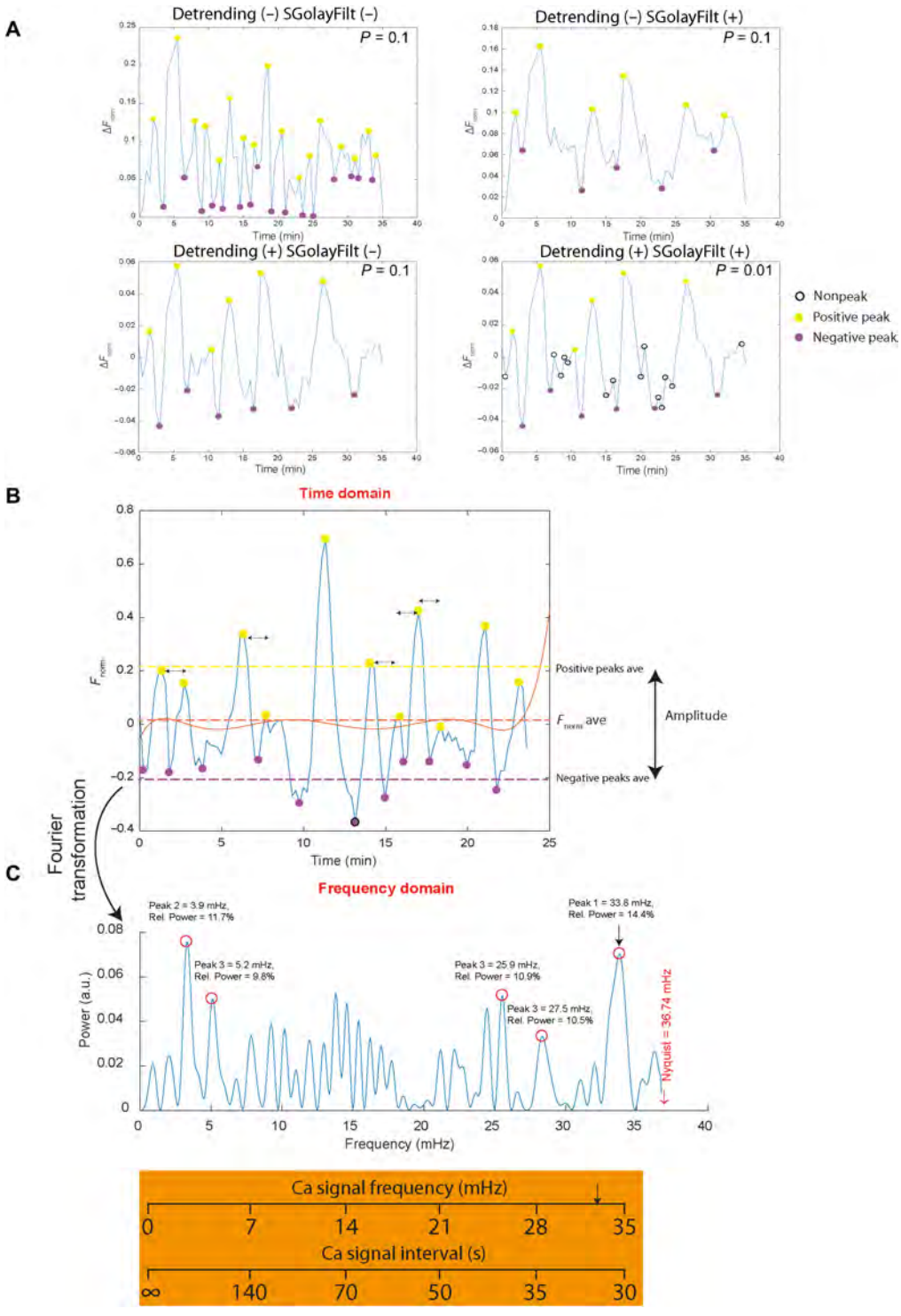

Fig. 2. Ca^{2+} signal analysis in vivo. (**A**) Representative mean fluorescence intensity time plot of a tissue-resident macrophage showing how the systematic and successive steps of detrending and filtering uncover oscillatory patterns. (**B**) A representative mean fluorescence intensity time plot of a tissue-resident macrophage displaying the basic parameters used to characterize Ca^{2+} signals in the time domain. (**C**) Top: PSD of the plot shown in (B) resulting from its Fourier transformation into the frequency domain displaying the five most dominant frequencies (red circles) and the most dominant one among them (arrow). Bottom: A frequency-to-period conversion tool, with the black arrow corresponding to the most dominant frequency.

(Fig. 4C). We also plotted macrophage distance from the site of laser injury against Ca^{2+} fluorescence intensity, which showed an exponentially inverse relationship between the two (Fig. 4C). Similar spatial-dependent activation in neutrophils was observed in terms of average Ca^{2+} signal intensity, signal amplitude, and PSD (Fig. 4D and movie S5). In addition, we observed a greater number of Ca^{2+} bursts in peritoneal macrophages in vitro after activation with HMGB1 than were observed before the application of HMGB1. This finding was consistent with a greater power after injury in the PSD, which is indicative of activation in terms of increased amplitude across the whole frequency spectrum (Fig. 4E). Furthermore, we investigated the effect of blockers of important Ca^{2+} regulators (SKF-96365 against STIM1, TRPCs, and other Ca^{2+} channels; 3-(6-methoxybenzo[d][1,3]dioxol-5-yl)-8,8-dimethyl-4H,8H-pyrano[2,3-f] chromen-4-one (AnCoA4) particularly against Orai1; and larixyl acetate particularly against TRPC6) on peritoneal macrophages stimulated by IL-1β in vitro. In comparison to cells incubated with dimethyl sulfoxide (DMSO) as a negative control, all of the inhibitor-treated cells showed a significant reduction in the amplitudes of their Ca^{2+} signals, whereas the inhibitors had no observed effects on normalized intensity and dominant frequency (Fig. 4F). In terms of PSD spectra, a general reduction in the area under the curve was observed for all of the blockers. Furthermore, each blocker led to a distinct spectral signature: The broad inhibitor SKF-96365 resulted in a decreased PSD across the whole frequency spectrum, whereas AnCoA4 mainly decreased higher frequencies and larixyl acetate only affected certain frequencies while not affecting the overall pattern (Fig. 4G). Hence, application of our Ca^{2+} imaging system enabled us to reveal that tissue-resident macrophages reacted to sterile inflammation in a manner dependent on their distance from the site of injury (Fig. 4H) even before neutrophils were recruited from the blood stream.

Downloaded from https://www.science.org at University Montpellier on September 11, 2023

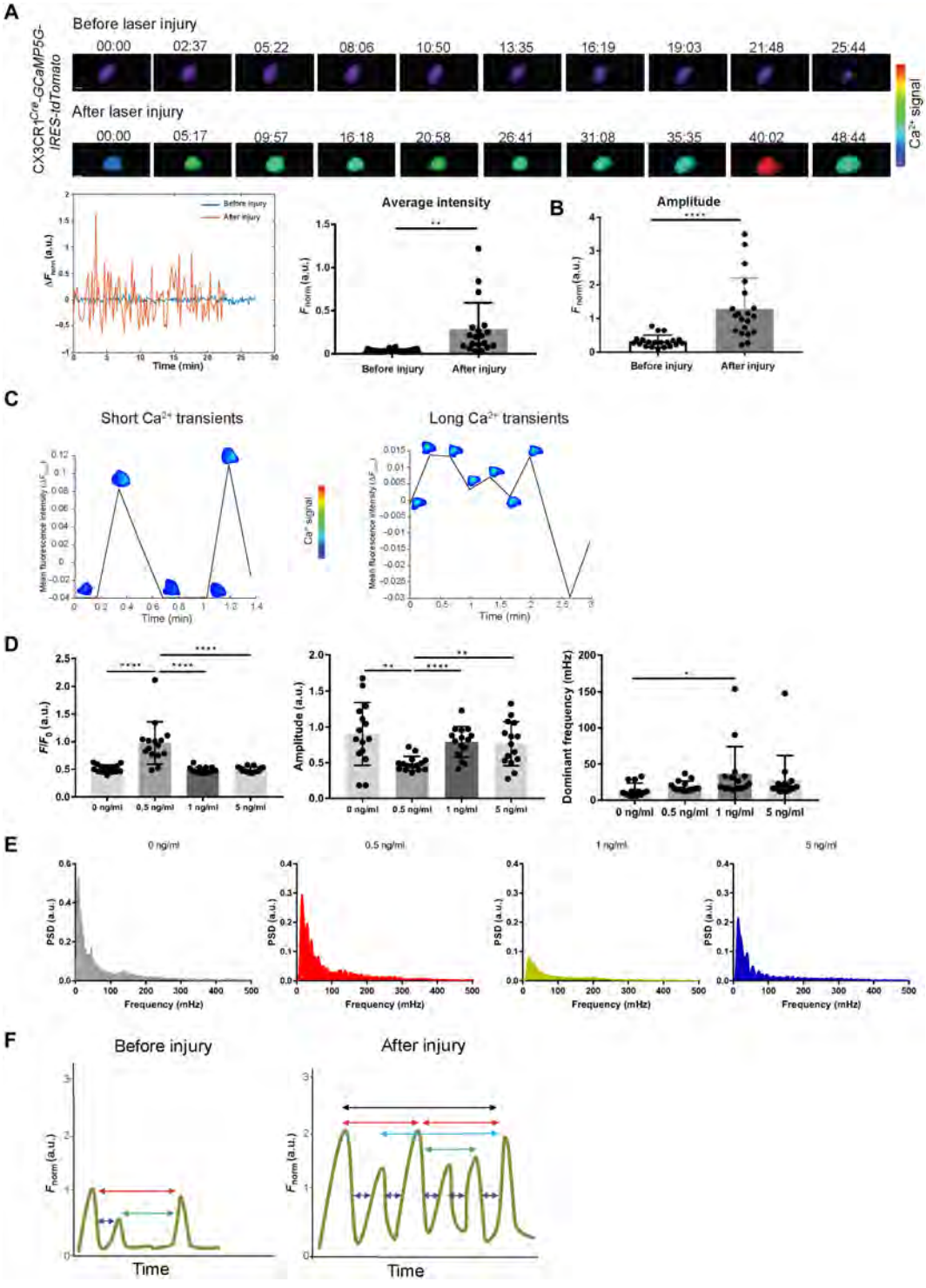

Fig. 3. Activation of tissue-resident macrophages by tissue necrosis. (**A**) Top: Representative time-lapse images of the Ca^{2+} signal of tissue-resident macrophage in pseudocolored mode before and after laser injury. Scale bars, 10 μm. Time is indicated in min:s. Bottom: Mean fluorescence intensity time plot tracings of the normalized Ca^{2+} signal of the cell before and after laser injury (left) and average mean fluorescence intensity of tissue-resident macrophages before and after laser injury (right). Data are means ± SEM of three to five mice per group and were analyzed by unpaired *t* test. $^{**}P \leq 0.01$. (**B**) Ca^{2+} signal amplitudes of tissue-resident macrophages before and after laser injury. Data are means ± SEM of three to five mice per group and were analyzed by unpaired *t* test. $^{****}P \leq 0.0001$. (**C**) Mean fluorescence intensity time plot of tissue-resident macrophages displaying short (left) and long (right) Ca^{2+} transients. Images of the Ca^{2+} signals of the cells in pseudocolored mode are transposed onto the plots. (**D**) Normalized intensity (left), amplitude (middle), and dominant frequency (right) of tissue-resident macrophages after stimulation with the indicated concentrations of IL-1β. Data are means ± SEM of 15 cells per group and were analyzed by unpaired *t* test. $^{*}P \leq 0.05$, $^{**}P \leq 0.01$, and $^{****}P \leq 0.0001$. (**E**) PSD plots of tissue-resident macrophages after stimulation with the indicated concentrations of IL-1β. (**F**) Representative summary of the data. Mean fluorescence intensity time plots of a tissue-resident macrophage before (left) and after (right) laser injury showing differences in Ca^{2+} signal parameters. Arrows of different colors correspond to different periods and frequencies.

Distinct Ca^{2+} signal patterns are observed during neutrophil recruitment stages in vivo

Having characterized the Ca^{2+} signals in immotile macrophages by two-photon microscopy at a cellular level, we then wanted to assess Ca^{2+} dynamics in migrating neutrophils. We performed intravital SDCM analysis of the cremaster muscle after *N*-formyl-Met-Leu-Phe (*f*MLP) injection, which provided a subcellular spatial resolution and a temporal resolution in the range of milliseconds. This procedure enabled us to determine Ca^{2+} dynamics during the leukocyte recruitment cascade in $LysM^{Cre}$-*GCaMP5G-IRES-tdTomato*$^{fl/fl}$ mice in vivo. During the rolling of neutrophils on the endothelium, the highest intensity of the Ca^{2+} signal was found in the center and on the endothelial cell–contacting side of the neutrophils (Fig. 5A and movie S6). To observe whether the nucleus had any displacing

Downloaded from https://www.science.org at University Montpellier on September 11, 2023

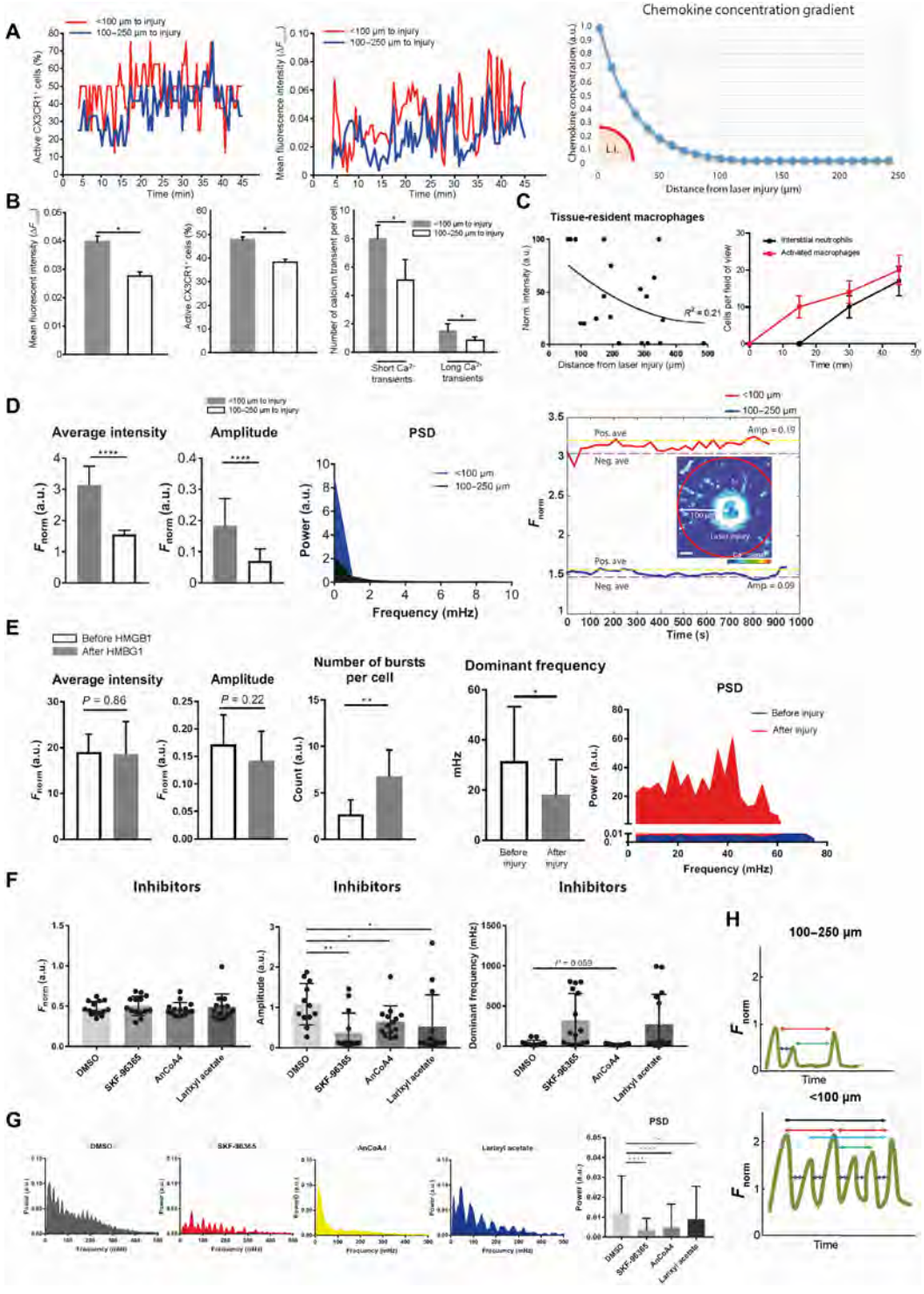

Fig. 4. The activation state of myeloid leukocytes depends on their distance from the site of injury. (**A**) Representative temporal distribution and mean fluorescence intensity time plots of active tissue-resident macrophages within a 100-µm radius of the site of laser injury versus those cells farther from the site. Right: Theoretical representation of the chemokine spatial concentration gradient that is released from the site of laser injury (L.I.) in the mouse skin model. The highest and lowest chemokine concentrations are represented by 1.0 and zero, respectively. (**B**) Average Ca^{2+} fluorescence intensity of tissue-resident macrophages, percentage of active tissue-resident macrophages, and number of Ca^{2+} transients per tissue-resident macrophage within a 100-µm radius of the site of laser injury compared to those of cells 100 to 250 µm from the site. Data are means ± SEM of five mice per group and were analyzed by unpaired *t* test. $^{*}P \leq 0.05$. (**C**) Left: Distance-dependent activation of tissue-resident macrophages. Normalized intensity values of tissue-resident macrophages from five mice were adjusted from 0 (lowest) to 100 (highest) within each mouse and plotted on the same graph as a function of the distance of the cells from the site of laser injury. A quadratic regression line was used to fit the data points. Right: Temporal comparison of the activation of tissue-resident macrophages compared to that of interstitial neutrophils in response to a laser injury set in the mouse skin model. Data are means ± SEM of three mice per group. (**D**) Average Ca^{2+} fluorescence intensity, amplitude, PSD, and intensity time plot of neutrophils within a 100-µm radius of the site of laser injury versus those 100 to 250 µm from the site. Data are means ± SEM of 14 or 18 cells per group and were analyzed by unpaired t test. $^{****}P \leq 0.0001$. The inset image in the intensity time plot shows neutrophils in the vicinity of the laser injury in a *LysM*^{Cre}-*GCaMP5G-IRES-tdTomato*$^{fl/fl}$ mouse. Scale bar, 20 µm. (**E**) Average intensity, amplitude, and number of Ca^{2+} transients per cell in peritoneal macrophages during a 10-min period after HMGB1 treatment in vitro. Data are means ± SEM of 12 cells per group and were analyzed by unpaired *t* test. Dominant frequency and PSD plot of tissue-resident macrophages from CX3CR1^{Cre}-*GCaMP5G-IRES-tdTomato*$^{fl/fl}$ mice before and after laser injury in vivo. Data are means ± SEM of three to five mice per group and were analyzed by unpaired *t* test. $^{*}P \leq 0.05$ and $^{**}P \leq 0.01$. (**F**) Normalized intensity, amplitude, and dominant frequency of peritoneal macrophages pretreated with DMSO, SKF-96365, AnCoA4, or larixyl acetate and then incubated with IL-1β (1 ng/ml). Data are means ± SEM of three mice per group and were analyzed by unpaired *t* test. $^{*}P \leq 0.05$ and $^{**}P \leq 0.01$. (**G**) PSD plots of peritoneal macrophages that were pretreated with DMSO, SKF-96365, AnCoA4, or larixyl acetate and then incubated with IL-1β (1 ng/ml). Right: Average PSD value over every frequency point (1 to 500 mHz) for the indicated treated peritoneal macrophages. Data are means ± SEM of three mice per group and were analyzed by unpaired *t* test. $^{**}P \leq 0.01$, $^{****}P \leq 0.0001$. (**H**) Representative summary of the data. Mean fluorescence intensity time plots of a tissue-resident macrophage within a 100-µm radius of the site of laser injury compared to that of cell farther from the site showing differences in Ca^{2+} signal parameters. Arrows of different colors correspond to different periods and frequencies.

Downloaded from https://www.science.org at University Montpellier on September 11, 2023

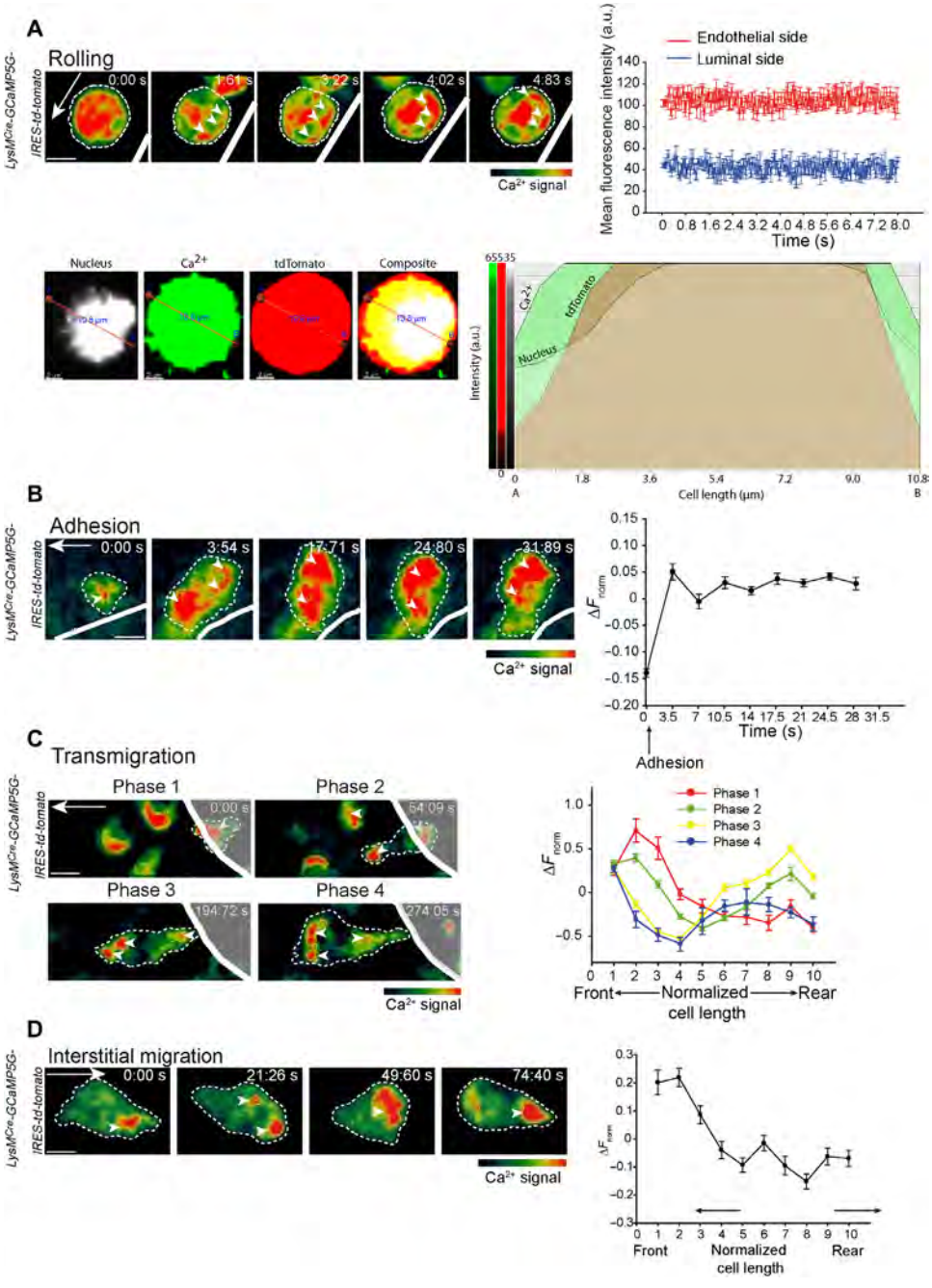

Fig. 5. Intracellular Ca^{2+} dynamics of neutrophils during the recruitment and migration cascade. (**A**) Top left: Time-lapse images of a neutrophil rolling along the endothelial wall in the cremaster muscle showing its spatiotemporal Ca^{2+} signal distribution in pseudocolored mode. The arrow indicates the overall direction of flow, the white solid line shows the vessel wall, and the arrowheads indicate regions of high Ca^{2+} concentration. Scale bar, 10 μm. Time is indicated in s:ms. Top right: Fluorescence intensity time plot of neutrophil Ca^{2+} signal showing the signaling intensities on the endothelial and luminal sides of cells. Data are from 20 cells and are representative of four mice. Bottom: Nuclear staining, Ca^{2+} signal, constitutive tdTomato signal, and composite picture of a rolling neutrophil (left), as well as intensity line profiles of the three different channels (right). (**B**) Left: Time-lapse images of a neutrophil adherent on the endothelial wall in the cremaster muscle showing its spatiotemporal Ca^{2+} signal distribution in pseudocolored mode. The arrow indicates the overall direction of flow. Scale bar, 10 μm. Time is indicated in s:ms. Right: Mean fluorescence intensity time plot of the Ca^{2+} signal of the neutrophil from the point of adhesion, which is indicated by the arrow. Data are from 14 cells and are representative of four mice. (**C**) Left: Time-lapse images of a neutrophil transmigrating through the endothelial wall in the cremaster muscle with its spatiotemporal Ca^{2+} signal distribution in pseudocolored mode and depicting phases 1 to 4 of the transmigration process. The arrow indicates the overall direction of migration. Scale bar, 10 μm. Time is indicated in s:ms. Right: Mean fluorescence intensity profile across the length of a transmigrating neutrophil normalized to the direction of migration, where 10 is the lagging edge and 1 is the leading edge. Each of the four successive stages of the transmigration process is depicted by its mean profile with a distinct color bound by 95% confidence intervals (dashed lines). Data are from 13 cells and are representative of four mice. (**D**) Left: Time-lapse images of a neutrophil migrating through the interstitial space in the cremaster muscle with its spatiotemporal Ca^{2+} signal distribution in pseudocolored mode. The arrow indicates the overall direction of migration. Scale bar, 10 μm. Time is indicated in s:ms. Right: Mean fluorescence intensity profile across the length of an interstitially migrating neutrophil (normalized to direction of migration, where 10 is the lagging edge and 1 is the leading edge). The migration process is depicted by its mean profile bound by 95% confidence intervals (dashed lines). Data are from 18 cells and are representative of four mice.

effect on intracellular Ca^{2+}, we first checked the viability of our chosen nuclear stain on $LysMeGFP^+$ cells in the absence of any stimulant or flow at a high magnification rate (movie S7). Because we were convinced of the nuclear staining protocol from the globular shapes of the nuclei as expected for neutrophils, we further stained the nuclei of the neutrophils and placed them under flow in a chamber coated with P-selectin, intercellular adhesion molecule, and CXCL1 to initiate adhesion and rolling. In rolling cells, we observed that the nuclear stain colocalized with the Ca^{2+} signal, indicating that the nucleus did not displace intracellular Ca^{2+} (Fig. 5A and movie S8). During firm adhesion, neutrophils exhibited an increase in Ca^{2+} signal in the whole cell, which changed to a polarized pattern to the front when transmigration was initiated in the intravascular compartment (phase 1; Fig. 5, B and C, and movie S9). During transmigration, the Ca^{2+} signal remained polarized; when the neutrophils extended protrusions from the blood stream into the interstitial space (phase 2) and when they reached the interstitial space (phase 3), they exhibited increased Ca^{2+} signal intensity at the leading and trailing

Downloaded from https://www.science.org at University Montpellier on September 11, 2023

edges. After they arrived in the interstitial space, the neutrophils exhibited a Ca^{2+} signal that was polarized to the lamellipodium (phase 4), which remained during interstitial migration with a polarization in the direction of migration (Fig. 5, C and D, and movies S10 and S11). At this stage, there was no direct correlation between the instantaneous change in normalized Ca^{2+} signal intensity and the change in cell speed or direction of interstitial cell migration (fig. S2, A and B). In summary, the distribution of Ca^{2+} signals and frequency spectrum in neutrophils depended on the stage of the leukocyte recruitment cascade (movie S12).

Effects of Orai1 on neutrophil Ca^{2+} dynamics and migration patterns in vivo

Because $G\alpha_i$-coupled GPCRs initiate leukocyte Ca^{2+} signals in vitro, we tested whether, with our experimental setup, we could detect the influence of inhibiting the signaling of these receptors in vivo. Therefore, we assessed how pertussis toxin (PTx), which blocks the activation of $G\alpha_i$ G proteins and inhibits leukocyte migration, affected Ca^{2+} signaling in neutrophils in vivo using the inflamed cremaster muscle model in *LysM^{Cre}-GCaMP5G-IRES-tdTomato$^{fl/fl}$* reporter mice (Fig. 6A and fig. S3A).

During the first stage of the cascade, the rolling fraction was unaffected by PTx (fig. S3B). The number of transmigrated neutrophils at various times after adoptive transfer was no different between control and PTx-treated groups (fig. S3B). However, the number of adherent cells in total and as a fraction of the total intravascular neutrophil population was increased as a result of PTx treatment (Fig. 6B). PTx resulted in reduced Ca^{2+} signal intensities and amplitudes in rolling cells in comparison to those in untreated neutrophils. PTx also resulted in a smaller dominant frequency, resulting in longer transients (Fig. 6C). However, once rolling cells had arrested, PTx resulted in no significant differences in Ca^{2+} signaling parameters (fig. S3C). In the second half of the migration cascade, the transmigration process appeared to be unaffected by PTx (fig. S3C). Once they entered the interstitial space, PTx-treated neutrophils displayed increased Ca^{2+} signal amplitudes compared to those of their control counterparts during migration but showed no change in average intensity or dominant frequency, and migratory parameters remained unaffected (Fig. 6D).

To further analyze differences in the signals between control cells and PTx-treated cells that would not be reflected by classical parameters, we compared the PSD of the migratory stages of neutrophils from the two groups. The biggest difference was observed during rolling, the power falling substantially after PTx treatment (Fig. 7A). During interstitial migration, the area under the PSD curve remained unchanged, but PTx resulted in a shifting of the PSD curve toward the lower end of the frequency spectrum; that is, it caused longer oscillations. Adhesion and transmigration were not affected by PTx (Fig. 7A). In summary, treatment of cells with PTx reduced short Ca^{2+} transients while maintaining long Ca^{2+} transients. Moreover, marking 2.5 s of interpeak temporal spacing (equivalent to a frequency of 400 mHz) as a threshold between short and long transients, short transients were markedly reduced in amplitude by PTx, whereas that of longer transients was slightly increased (Fig. 7B). These data suggest that $G\alpha_i$-coupled GPCRs are implicated in the migration cascade of neutrophils, which was reflected by the change in Ca^{2+} frequency spectra.

To characterize the effects of other specific Ca^{2+} signaling mechanisms in neutrophils, we treated bone marrow–derived Ca^{2+} reporter neutrophils with AnCoA4 (an Orai1 inhibitor), SKF-96365 (a STIM1 inhibitor), or DMSO (control) and performed chemotaxis assays in vitro. In terms of classical migratory parameters, we analyzed the total accumulated distance, the Euclidean distance, and the velocity of neutrophils during chemotaxis. Only AnCoA4 resulted in a significant reduction in all three parameters in comparison to DMSO (fig. S3D). Similarly, this effect was observed in the PSD spectra, whereby AnCoA4-treated cells had a greater area under the curve than did cells treated with DMSO or SKF-96365 (Fig. 7C). Last, AnCoA4 did not affect either Ca^{2+} signal intensity or amplitude, whereas SKF-96365 resulted in a significant decrease in only mean fluorescence intensity (fig. S3E). Because AnCoA4 showed an effect in vitro, we further investigated its role in the neutrophil migration cascade by adapting the in vivo neutrophil adoptive transfer scheme that we used to test the effects of PTx. In the resulting PSD spectra, we observed that Orai1 inhibition affected the neutrophil Ca^{2+} signal during rolling, adhesion, and interstitial migration (Fig. 7D). During adhesion, the PSD was substantially decreased after Orai1 inhibition, whereas during interstitial migration, higher frequencies were blunted. This was accompanied by reductions in the number of adherent cells, the mean fluorescence intensity of their Ca^{2+} signal, and track straightness during interstitial migration, and an increase in the mean fluorescence intensity of the Ca^{2+} signal during interstitial migration as a result of Orai1 inhibition (Fig. 7E). The rolling velocity, number of transmigrating cells, and velocity during interstitial migration were unaffected (fig. S4A). Moreover, Ca^{2+} signal mean fluorescence intensity during rolling and transmigration and Ca^{2+} signal amplitude in all stages of the recruitment cascade were unaffected by AnCoA4 (fig. S4, B and C). Thus, we provide evidence that inhibition of Orai1 resulted in changes in Ca^{2+} signals during adhesion and interstitial migration, which were connected to changes in cell behavior.

DISCUSSION

The current knowledge about Ca^{2+} signaling in myeloid leukocytes comes mainly from studies involving dye-loaded cellular in vitro imaging techniques. Here, in vivo imaging of transgenic Ca^{2+} reporter mouse strains enabled us to detect Ca^{2+} oscillations in tissue macrophages after sterile injury and to identify distinct Ca^{2+} signal patterns in neutrophils at each migration cascade step. Having looked at the first layer of Ca^{2+} signaling in neutrophils, we confirmed the involvement of PTx-sensitive GPCRs in neutrophil activation during the migration cascade, whereas inhibition of Orai1 provided a link between alterations in Ca^{2+} signals and changes in neutrophil migration (figs. S5 and S6). These findings are based on classical Ca^{2+} signaling parameters being coupled to a comprehensive spectral method for the assessment of complex Ca^{2+} signals in vivo.

The Cre-dependent *GCaMP5G-IRES-tdTomato* reporter mouse was used by Gee *et al.* (*36*) in a study of neurons and glial cells in vivo. The authors used the constitutive tdTomato signal as an indicator of cells that exhibited low levels of Ca^{2+} signaling. Similarly, we were able to replicate this genetic labeling approach for our *LysM^{Cre}* and *CX3CR1^{Cre}* constructs in neutrophils and macrophages. The Ca^{2+} signal in dorsal root ganglion neurons operate in the frequency range of 200 to 2000 mHz, whereas immune cells, such as T lymphocytes, operate at a much lower frequency range of 0.5 to 200 mHz (*38*). Hence, the *GCaMP5G-IRES-tdTomato* reporter mouse enabled the detection of Ca^{2+} oscillations in tissue-resident

Downloaded from https://www.science.org at University Montpellier on September 11, 2023

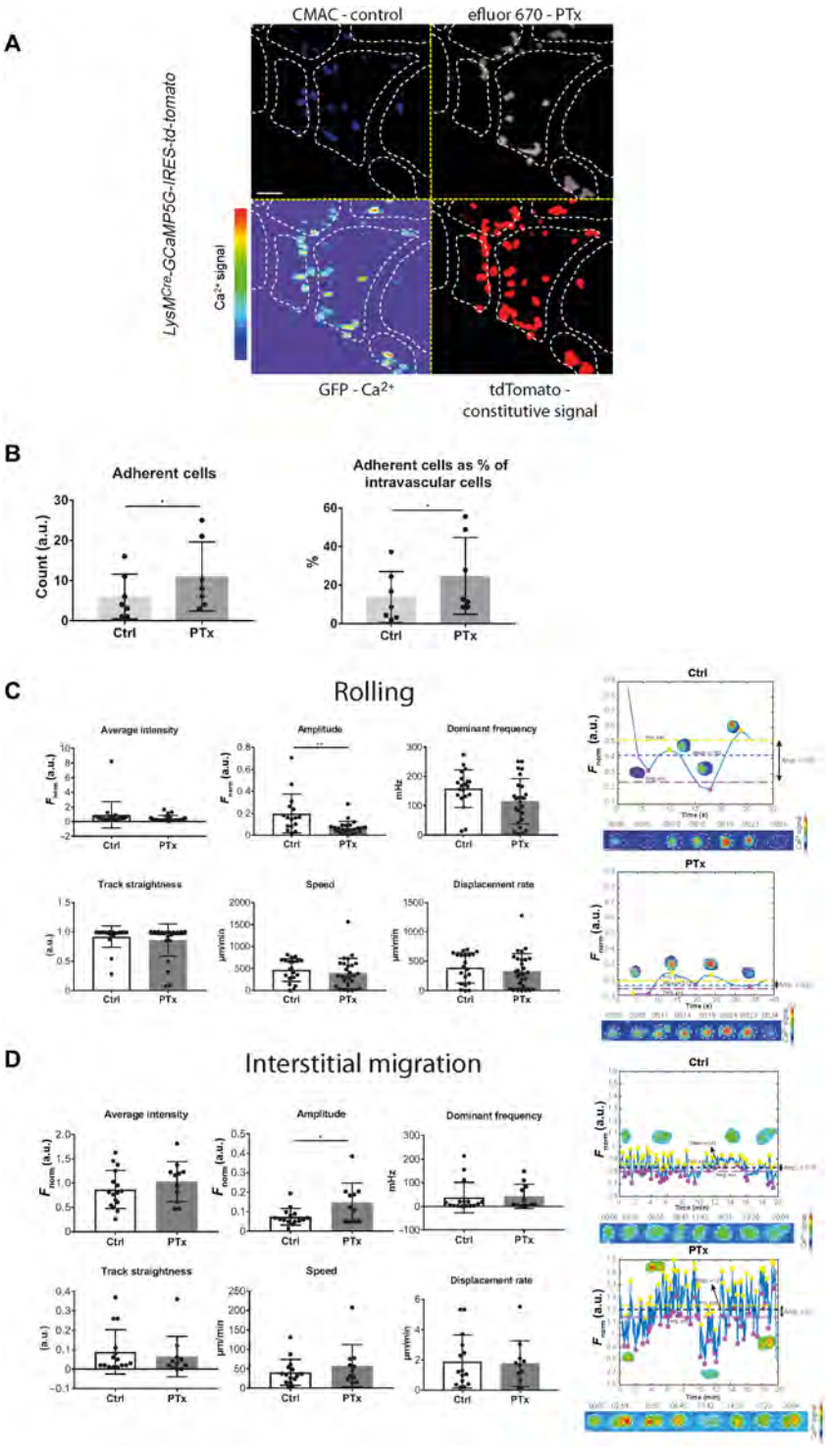

Fig. 6. Effects of PTx on Ca^{2+} signals in migrating neutrophils in vivo. (**A**) Adoptively transferred neutrophils imaged at all migration stages within the microvasculature of the cremaster muscle are displayed in blue for untreated control cells, gray for PTx-treated cells, pseudocolored for the intracellular Ca^{2+} signal, and red for the constitutive tdTomato signal. Still image is from SDCM analysis of the cremaster muscle in vivo. Scale bar, 30 μm. (**B**) Total number of adherent neutrophils and percentage of adhesion of all (intra- and extravascular) neutrophils 2 to 3 hours after induction of inflammation of adherent cells in control versus PTx-treated neutrophils after *f*MLP-induced inflammation. Data are means ± SEM of seven mice per group and were analyzed by unpaired *t* test. $*P \leq 0.05$. (**C**) Left: Ca^{2+} signal parameters (average intensity, amplitude and dominant frequency; top) and migration parameters (track straightness, speed, and displacement rate; bottom) of control and PTx-treated neutrophils during the rolling phase. Data are means ± SEM of four mice per group and were analyzed by unpaired *t* test. $**P \leq 0.01$. Right: Representative mean fluorescence intensity time plots and time-lapse images of neutrophils from the indicated treatment groups. Scale bars, 5 μm. Time is indicated in min:s. (**D**) Left: Ca^{2+} signal parameters (top) and migration parameters (bottom) of control and PTx-treated neutrophils undergoing interstitial migration. Data are means ± SEM of three or four mice per group and were analyzed by unpaired *t* test. $*P \leq 0.05$. Right: Representative mean fluorescence intensity time plots and time-lapse images of neutrophils from the indicated treatment groups. Scale bars, 5 μm. Time is indicated in min:s.

macrophages and neutrophils in the migration cascade in vivo covering the ranges 20 to 40 mHz and 20 to 150 mHz, respectively.

Gee *et al.* (*36*) focused on normalized signal intensity, number of spikes, and frequency, which was evaluated as the number of spikes per minute for their analysis of Ca^{2+} signals and dynamics, similarly to many other studies with in vitro and in vivo Ca^{2+} signaling data. However, these classical parameters do not capture the full complexity of highly irregular Ca^{2+} signals in vivo. This limitation can be overcome by spectral analysis of Ca^{2+} signal oscillations. The spectral method makes use of the normalized signal intensity to transition from the time domain into the frequency domain by Fourier transformation. The PSD is a representation of the power of one frequency in a spectrum relative to the combined power of all of the other frequencies; hence, it is also referred to as the relative power. Power is a measure of the squared amplitude of the signal and, hence, also the activation of the cells. Therefore, graphs of PSD against frequency primarily reveal the order of significance of a signal's frequencies and secondarily hint at a signal's amplitude. It is evident from PSDs that there are a multitude of frequency values above the noise threshold, highlighting that Ca^{2+} signals in vivo are not just a mere one-frequency phenomenon but rather are made of multiple frequencies that would be difficult to identify within the time domain. Therefore, the spectral method has an advantage compared to the classical analysis of events per minute because it offers insight into a broad range of frequency values as opposed to just a single value.

Resident-tissue macrophages perform the endocytosis and phagocytosis of bacterial infection debris in a Ca^{2+}-dependent manner (*39*). We therefore wanted to explore whether this was also the case during nonpathogenic tissue damage, and we found that Ca^{2+} signal intensity in macrophages was significantly increased after induction of sterile inflammation by a laser injury. Moreover, Ca^{2+}

Downloaded from https://www.science.org at University Montpellier on September 11, 2023

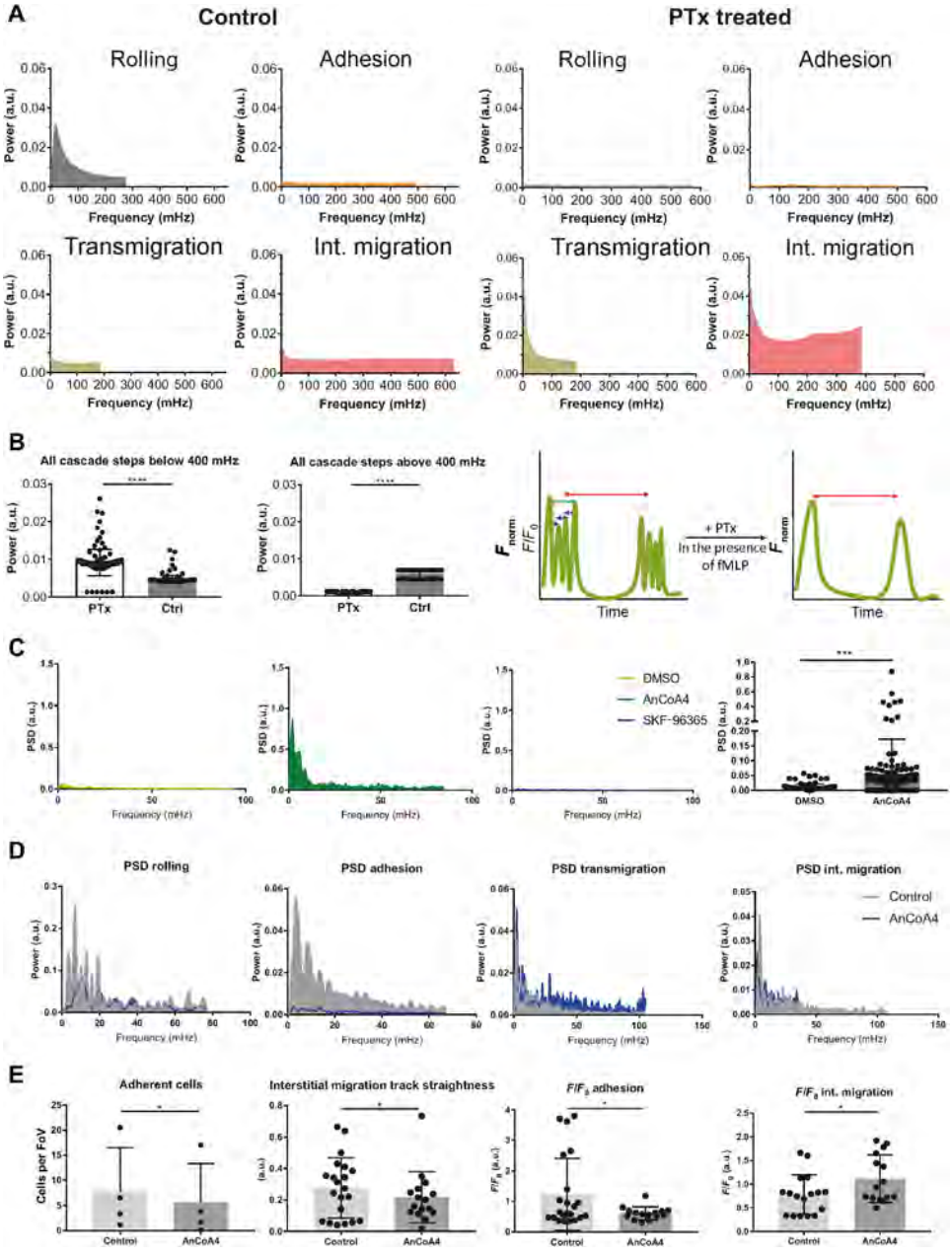

Fig. 7. Gα_i-coupled GPCR– and Orai1-dependent Ca^{2+} signals in migrating neutrophils in vivo. (**A**) PSD plots of the indicated recruitment stages of control (left) and PTx-treated (right) neutrophils from *LysM*^{Cre}*-GCaMP5G-IRES-tdTomato*$^{fl/fl}$ reporter mice that were adoptively transferred into male C57BL/6 mice, whose cremaster muscle had already been inflamed and then was imaged by SDCM. (**B**) Left: Average power values of <400 and >400 mHz as calculated from PSD plots with all migration stages combined for control and PTx-treated neutrophils. Data are means ± SEM of four mice per group and were analyzed by unpaired *t* test. ****$P \leq 0.0001$. Right: Representative summary mean fluorescence intensity time plots of a neutrophil showing the effects of PTx on short and long transients. Arrows of different colors correspond to different periods and frequencies. (**C**) Left: PSD plots of neutrophil chemotaxis in vitro after treatment with DMSO (control), AnCoA4, or SKF-96365. Data are from three mice per group. Right: Average PSD value over every frequency point (1 to 100 mHz) for chemotactic neutrophils after treatment with DMSO (control) and AnCoA4. Data are means ± SEM of three mice per group and were analyzed by unpaired *t* test. ***$P \leq 0.001$. (**D**) PSD plots of adoptively transferred neutrophils in vivo after AnCoA4 treatment during the indicated four transmigration cascade steps. (**E**) Average numbers of adherent cells, average track straightness of interstitially migrating cells, mean fluorescence intensity of adherent cells, and mean fluorescence intensity of interstitially migrating cells were compared for control and AnCoA4-treated neutrophils injected into the same mouse in which cremaster inflammation was induced by *f*MLP. Data are means ± SEM of four mice per group and were analyzed by unpaired *t* test. *$P \leq 0.05$. FoV, field of view.

signal analysis enabled us to uncover that tissue macrophages closer to the center of the site of necrosis were activated earlier and more intensively than those further away from the site of damage. This could be due to the greater concentration of DAMPs in the vicinity of the necrotic area.

Moreover, neutrophils exhibit a different type of Ca^{2+} signal compared to that of macrophages. Beerman *et al.* (*23*) showed that during the migration of neutrophils in zebrafish toward a tissue injury, the leading edge of the neutrophil has the greatest Ca^{2+} signal intensity, as was the case with our study of neutrophils during transmigration and interstitial migration in mice. This cell context–dependent variability in the range of intracellular Ca^{2+} spikes is thought to be a way in which cells encode different types of stimuli (*40*). Comparably, we showed that neutrophils exhibited markedly different frequency signatures depending on which stage of the cascade they were in, as well as while executing effector functions at the site of necrosis, adding to the notion that Ca^{2+} signal spectra reflect different functional states of the cell.

PTx inhibits intracellular Ca^{2+} signaling in myeloid leukocytes downstream of Gα_i-coupled GPCRs and thereby inhibits their chemotactic response, but how Ca^{2+} signals are affected in vivo is unclear (*41*, *42*). Such GPCRs cooperate with calcium release-activated channels (CRAC) to stimulate intracellular Ca^{2+} flux, resulting in the arrest and polarization of neutrophils (*10*). Furthermore, Ca^{2+} flux causes neutrophil arrest by initiating lymphocyte function associated antigen 1 (LFA-1) clustering (*43*). We therefore chose PTx, which blocks the activation of Gα_i G proteins, to test our in vivo Ca^{2+} signaling characterization method.

Ca^{2+} signaling is an inherent part of the neutrophil recruitment cascade as myeloid leukocytes leave the vasculature and arrive at a target site. Outside-in signaling mechanisms, which are responsible for leukocyte rolling and arrest, depend on Gα_i-coupled GPCRs (*44*, *45*). Correspondingly, we showed that the PSD of rolling was markedly reduced upon PTx treatment, whereas that of interstitial migration increased. Moreover, PTx caused an increase in the amount

Downloaded from https://www.science.org at University Montpellier on September 11, 2023

and proportion of neutrophils that adhered to the endothelium. Consistent with our finding in mice, PTx treatment in rats also results in increased leukocyte adhesion to the vessel wall (*46*). During rolling, intracellular Ca^{2+} stores from the endoplasmic reticulum (ER) are released into the cytoplasm through other receptor pathways. The lack of effect of PTx on migratory or Ca^{2+} signaling parameters during adhesion and transmigration may be explained by the involvement of other intracellular Ca^{2+} regulation mechanisms, such as SOCE- and Orai1-mediated Ca^{2+} uptake and release during these stages of the cascade (fig. S6). Orai1 is the main regulator of SOCE in neutrophils, and its inhibition decreases the bactericidal function and the arrest and migration of neutrophils (*10*, *47*, *48*). Consistent with this, inhibition of Orai1 had a distinct effect on neutrophil migration by decreasing neutrophil adhesion and changing the pattern of interstitial migration, which was linked to a change in PSD and mean fluorescence intensity during these stages of leukocyte migration in vivo. This intersection of effects on cellular migration and Ca^{2+} signal modalities highlights the effectiveness of our analysis, which is based on a well-characterized Ca^{2+} channel-inhibitor axis. Whereas the classical normalized intensity parameter fails to show the importance of the reduction in neutrophil activation during rolling, the PSD shows how $G\alpha_i$-coupled GPCRs and Orai1 affect Ca^{2+} signal spectra in neutrophils in vivo. Given that the PSDs of Ca^{2+} signal spectra integrate many aspects of information within the various frequency values, an additional analysis or a combination with other fluorescent reporters of signaling molecules would need to be performed to fully grasp the extent of biological information that can be extracted from these and similar experiments.

The Ca^{2+} signaling analysis algorithm presented here provides an opportunity to examine many more cell types than neutrophils and macrophages in their native environments. This can be done not only in settings of sterile and microbial inflammation but also to answer any other biologically relevant question provided that one can generate the necessary setting in the proper Ca^{2+} reporter mouse strain. Nevertheless, this technique only analyzes local interplays and should therefore be combined with other systemic models. The strength of this analysis technique lies in the endogenous labeling of Ca^{2+}, thus removing the need for dyes to label Ca^{2+} signaling. On the other hand, for this intravital analysis technique to be successful, one needs to have access to equipment such as a two-photon intravital microscopy and an SDCM; however, there have been advancements resulting in the generation of GCaMP fusion proteins with stronger fluorescence that may facilitate a more universal use of this tool and help overcome the inherent limitation of this mouse model (*49*). The versions of the protein fusion known as GCaMP6f and GCaMP7f enhance Ca^{2+} signal intensity by more than three times that of GCaMP5g and lead to half-decay times of 140 ± 430 ms and 265 ± 20 ms, respectively (*50*). Last, note that Ca^{2+} signaling is just one of various cell signaling processes, and one should therefore combine it with fluorescent reporters for other signaling molecules.

With our spectral method of investigating Ca^{2+} dynamics in vivo, we provide a method for assessing leukocyte activation. Coupled to the Cre-lox recombination system, which enables the GCaMP5G-IRES-tdTomato reporter to be expressed in any cell line, a plethora of opportunities open up for further characterizations of Ca^{2+} signal–based activation in vitro and in vivo. Ca^{2+} signaling was previously suggested as a key mechanism to target in the fight against various autoimmune and inflammatory immune diseases (*51*). Our findings increase our understanding of how alterations in Ca^{2+} signals are linked to changes in cell behavior in vivo. First, each step of the neutrophil migration cascade was connected to a distinct pattern of Ca^{2+} signals, which we showed by applying PSD analysis. Second, the activation of macrophages in the context of sterile inflammation was assessed by intravital Ca^{2+} imaging, which showed an effect that was dependent on the distance from the site of injury. Third, inhibition of Orai1 was linked to alterations in Ca^{2+} signals and changes in cell behavior in vivo. Our approach adds to this effort by establishing previously unknown opportunities to analyze the responses of leukocytes (or any immune cells given the ubiquitous nature of Ca^{2+} signaling) to therapeutic interventions in vivo. This not only provides an opportunity to develop ways of analyzing leukocytes in vivo but also warrants the need for linking different Ca^{2+} flux signatures with distinct cellular programs.

MATERIALS AND METHODS

Mice

All mice were maintained and crossbred in the specific pathogen–free animal facility of the Walter Brendel Centre of Experimental Medicine at the Ludwig-Maximilians-Universität Munich. All procedures performed on mice were authorized by the local legislation on protection of animals (Commission on Animal Protection, 55.2.1.54-2532-23-12 and 55.2-2532.Vet_02-19-42, Regierung von Oberbayern, Munich). C57BL/6NCrl mice were bought from Charles River Laboratories. For intravital visualization, heterozygous *CX3CR1*$^{eGFP/+}$ were used (*52*, *53*). *B6;129S6-Polr2atm1(CAG-GCaMP5g-tdTomato)Tvrd/J* (*GCaMP5G-IRES-tdTomato*$^{fl/fl}$) were purchased from the Jackson Laboratory and crossbred in our animal facility with *LysM*^{Cre} or *CX3Cr1*^{Cre} mice. Mice used in experiments were at ages 8 to 12 weeks. Groups were age- and sex-matched and on a C57BL/6 background.

Intravital two-photon imaging

For intravital two-photon imaging, a tail vein catheter was inserted into mice after sedation with midazolam (5 mg/kg body weight; Hameln), medetomidine (0.5 mg/kg body weight; Pfizer), and fentanyl (0.05 mg/kg body weight; Albrecht) administered intraperitoneally. The ear was fixed on a custom-built stage. All dyes and antibodies were administered through a tail vein catheter. A multiphoton TriM Scope II system (LaVision BioTec) connected to an upright Olympus microscope equipped with a Ti:Sa Chameleon Ultra II laser (690 to 1040 nm; Coherent) and a 16× water immersion objective [numerical aperture (NA) 0.8; Nikon] were used to generate a laser injury. Focusing the laser beam on a field of 42 μm by 42 μm until autofluorescence appeared resulted in a single necrotic focus. Imaging was performed with an excitation wavelength of 800 to 900 nm (depending on the fluorochromes used) in a frame of 559 μm by 559 μm with 515 × 515 pixels, a frame rate of 2/min, and a *z* step of 3 μm in a range of 30 μm (20 to 50 μm below the epidermis). Three-dimensional (3D) reconstruction and acquisition of tracking parameters were performed with Imaris software (Bitplane).

Cremaster muscle model

Surgical preparation of the cremaster muscle was performed as originally described (*54*). Mice were anesthetized as described earlier. Labeled cells were administered through a tail vein catheter. The cremaster muscle was inflamed 2 hours before surgery by intrascrotal injection of 50 μM *f*MLP. Imaging was performed with an upright

Downloaded from https://www.science.org at University Montpellier on September 11, 2023

spinning disk confocal microscope (Examiner Z1, Zeiss) with the confocal unit scanner CSU-X1 (Yokogawa Electric Corporation), a charge-coupled device (CCD) camera (Evolve, Photometrics), and a 20×/1.0 NA water immersion objective (Plan Apochromat, Zeiss). Videos were recorded using four lasers with excitation wavelengths of 405, 488, 561, and 640 nm at an average frame rate of five per minute.

Adoptive transfer of neutrophils

LysM^{Cre}-GCaMP5G-IRES-tdTomato$^{fl/fl}$ reporter mouse bone marrow was flushed out of the humerus, femur, and tibia with phosphate-buffered saline (PBS). The cells were then centrifuged, and the pellet was resuspended in PBS. The suspension was then fractionated on a 52/64/72% Percoll gradient, and the enriched neutrophil fraction was recovered at the interface of the 64 and 72% layers. Neutrophil purity was determined by fluorescence-activated cell sorting to be >99%. The population was then divided into two, one half being stained with CellTracker Blue CMAC dye and the other being stained with eFluor 670 dye and treated with PTx (0.5 μg/ml) and 5 μM AnCoA4 (1.9 μg/ml) by incubation at 37°C for 30 min. Samples of both cell populations (150 μl), adjusted to 5×10^6 cells/ml, were then intravenously coinjected, in separate syringes to avoid staining of one or the other group by the wrong dye, into a C57BL/6 mouse, whose cremaster muscle had already been inflamed.

3D chemotaxis

The analysis of migration in collagen gels was performed with Ibidi μ-Slide Chemotaxis 3D chambers as previously described (*55*, *56*). For a collagen gel (1.5 mg/ml), a gel-cell mixture with murine bone marrow–derived neutrophils (7.5×10^5 per sample) in 5 μl of adhesion medium [ADM; containing 1.2 mM Ca^{2+}, 1 mM Mg^{2+}, 0.25% bovine serum albumin, 0.1% glucose, and 20 mM Hepes (pH 7.4) in Hanks' balanced salt solution] was prepared by mixing the cells with 2 μl of 10× ADM and 9 μl of type I rat tail collagen (5 mg/ml). The neutrophil-collagen solution was applied to the middle channel of the 3D chamber and left at 37°C for 5 min for gelation. After application of mCXCL1 (100 ng/ml) in ADM to one reservoir of the chamber and incubation for 20 min at 37°C, time-lapse videos were recorded for 10 min with a frame rate of 14 s with a Plan Apochromat 10×/0.3 NA objective and the microscope setup described earlier (*57*). Migration analysis was performed offline with ImageJ software.

Isolation of peritoneal macrophages for microscopy

Sticky slide VI$^{0.4}$ Ibidi chambers were coated with poly-L-Lys M (50 μg/ml) and incubated at 37°C and in 5.1% CO_2. *LysM^{Cre}-GCaMP5G-IRES-tdTomato$^{fl/fl}$* mice were anesthetized by isoflurane inhalation and euthanized by cervical dislocation. A small patch of skin was carefully removed from the belly area, ensuring that the abdominal wall remained puncture-free. Cold PBS (5 to 10 ml) was injected into the peritoneum. The abdomen was gently massaged on both sides to generate a peritoneal macrophage suspension. The suspension was then slowly removed with the same cannula through the same hole through which it was injected and, after a centrifugation step, resuspended at 3×10^6 cells/ml in RPMI 1640 with 10% fetal calf serum. A 200-μl sample of this suspension was used to coat the Ibidi chambers, which were further incubated for 4 hours under the same conditions described earlier. For HMGB1 experiments, each slide was imaged for 10 min. Before imaging, the chambers were flushed out with fresh RPMI 1640 solution to remove any nonattached cells. The peritoneal macrophages were first imaged without any intervention and then were treated with HMGB1 (2 μg/ml). An automated inverted IX83 Olympus microscope with a UPlan 40×/1.0 or UPLSAPO-PH 100×/1.4 oil immersion objective (Olympus) and a cooled CCD camera (XM10, Olympus) was used to capture epifluorescence movies. The microscope was fitted with a stage incubator (37°C, humidified; Tokai Hit). For the IL-1β dose dependency experiments, IL-1β was added to the peritoneal macrophages at concentrations of 0.5, 1, and 5 ng/ml, and the cells were incubated at 37°C for 30 min and then imaged at 3 min per slide. For Ca^{2+} signal inhibition experiments, peritoneal macrophages were treated with IL-1β (1 mg/ml) and 5 μM AnCoA4 (1.9 μg/ml), 5 μM SKF-96365 (2.0 μg/ml), or larixyl acetate (1.95 μg/ml) for 30 min and imaged at 3 min per slide with an inverted Zeiss LSM 880 (×20/0.8 NA objective).

Semi-automated system for analyzing Ca^{2+} signals

Intravital microscopy videos were imported into Imaris (Bitplane), and myeloid leukocyte surfaces were rendered and segmented to determine the mean fluorescence intensity of the whole surface of a cell. The automation process was executed with MATLAB (R2017a). To begin with, a code was designed around the Excel sheet output from Imaris to generate another Excel sheet with two columns, namely, the detrended signal and time. The intermediate spreadsheet was then filtered in MATLAB to remove any detectable noise, and last, the peaks were selected from it (see the Supplementary Materials for the code used). The final sheet contains the normalized intensity (F_{norm}), the difference in normalized intensity (ΔF_{norm}), and the amplitude. Moreover, the final output also consists of signals with labeled positive and negative peaks over time. Ca^{2+} signals were converted from the time domain into the frequency domain with the MATLAB plugin Spectral Analysis (version 3.0) as described previously (*58*). The various parameters used are defined by the following equations

$$F_{norm} = \frac{\text{Green channel intensity}}{\text{Red channel intensity}} \quad (1)$$

$$\Delta F_{norm} = F_{norm}(t+1) - F_{norm}(t) \text{ (where } t \text{ denotes time)} \quad (2)$$

$$\text{Amplitude} = F_{norm_{ave}}{}^{pos} - F_{norm_{ave}}{}^{neg} \quad (3)$$

$$\text{Highest peak amplitude (HPA)} = \max(F_{norm}) - \min(F_{norm}) \quad (4)$$

$$\text{Minimum peak prominence (MPP)} = p * [\max(F_{norm}) - \min(F_{norm})] \text{ (where } p \text{ denotes percentage)} \quad (5)$$

Ca^{2+} signal analysis parameters

The filtered Ca^{2+} signal was quantified with several parameters. The first parameter for quantifying Ca^{2+} signals was the normalized fluorescence intensity, F_{norm} (Eq. 1), which is the value of the Ca^{2+}-dependent GFP signal originating from the GCaMP5G construct divided by that of the constitutive tdTomato signal. The difference in normalized intensity between consecutive time points is referred to as ΔF_{norm} (Eq. 2). Furthermore, we defined the difference between the averages of the normalized intensity of the positive and negative peaks as amplitude because the highly irregular nature of the Ca^{2+} signal in vivo did not allow the application of equations used for regular (for example, sine wave) signals (Eq. 3).

Downloaded from https://www.science.org at University Montpellier on September 11, 2023

Statistical analysis

For tracking data, Student's unpaired *t* test and analysis of variance (ANOVA)–least significant difference post hoc test were used. A *P* value <0.05 was considered to be statistically significant.

SUPPLEMENTARY MATERIALS

www.science.org/doi/10.1126/scisignal.abe6909
Figs. S1 to S6
Movies S1 to S12
Supplementary Codes S1 and S2
MDAR Reproducibility Checklist

View/request a protocol for this paper from *Bio-protocol*.

REFERENCES AND NOTES

1. S. Feske, Y. Gwack, M. Prakriya, S. Srikanth, S. H. Puppel, B. Tanasa, P. G. Hogan, R. S. Lewis, M. Daly, A. Rao, A mutation in Orai1 causes immune deficiency by abrogating CRAC channel function. *Nature* **441**, 179–185 (2006).
2. R. S. Lacruz, S. Feske, Diseases caused by mutations in ORAI1 and STIM1. *Ann. N. Y. Acad. Sci.* **1356**, 45–79 (2015).
3. C. Picard, C. A. McCarl, A. Papolos, S. Khalil, K. Luthy, C. Hivroz, F. LeDeist, F. Rieux-Laucat, G. Rechavi, A. Rao, A. Fischer, S. Feske, STIM1 mutation associated with a syndrome of immunodeficiency and autoimmunity. *N. Engl. J. Med.* **360**, 1971–1980 (2009).
4. M. Trebak, J. P. Kinet, Calcium signalling in T cells. *Nat. Rev. Immunol.* **19**, 154–169 (2019).
5. S. Feske, H. Wulff, E. Y. Skolnik, Ion channels in innate and adaptive immunity. *Annu. Rev. Immunol.* **33**, 291–353 (2015).
6. S. Abbasi, A. Abbasi, Y. Sarbaz, M. Janahmadi, Power spectral density analysis of purkinje cell tonic and burst firing patterns from a rat model of ataxia and riluzole treated. *Basic Clin. Neurosci.* **8**, 61–68 (2017).
7. E. Tibau, M. Valencia, J. Soriano, Identification of neuronal network properties from the spectral analysis of calcium imaging signals in neuronal cultures. *Front. Neural. Circuits* **7**, 199 (2013).
8. M. L. Muiesan, D. Rizzoni, R. Zulli, M. Castellano, G. Bettoni, E. Porteri, E. Agabiti-Rosei, Power spectral analysis of the heart rate in hypertensive patients with and without left ventricular hypertrophy: The effect of a left ventricular mass reduction. *J. Hypertens.* **16**, 1641–1650 (1998).
9. N. Demaurex, P. Nunes, The role of STIM and ORAI proteins in phagocytic immune cells. *Am. J. Physiol. Cell Physiol.* **310**, C496–C508 (2016).
10. U. Y. Schaff, N. Dixit, E. Procyk, I. Yamayoshi, T. Tse, S. I. Simon, Orai1 regulates intracellular calcium, arrest, and shape polarization during neutrophil recruitment in shear flow. *Blood* **115**, 657–666 (2010).
11. H. Zhang, R. A. Clemens, F. Liu, Y. Hu, Y. Baba, P. Theodore, T. Kurosaki, C. A. Lowell, STIM1 calcium sensor is required for activation of the phagocyte oxidase during inflammation and host defense. *Blood* **123**, 2238–2249 (2014).
12. R. Immler, S. I. Simon, M. Sperandio, Calcium signalling and related ion channels in neutrophil recruitment and function. *Eur. J. Clin. Invest.* **48**, e12964 (2018).
13. N. Dixit, S. I. Simon, Chemokines, selectins and intracellular calcium flux: Temporal and spatial cues for leukocyte arrest. *Front. Immunol.* **3**, 188 (2012).
14. B. A. Kruskal, S. Shak, F. R. Maxfield, Spreading of human neutrophils is immediately preceded by a large increase in cytoplasmic free calcium. *Proc. Natl. Acad. Sci. U.S. A.* **83**, 2919–2923 (1986).
15. G. Chen, D. Zhang, T. A. Fuchs, D. Manwani, D. D. Wagner, P. S. Frenette, Heme-induced neutrophil extracellular traps contribute to the pathogenesis of sickle cell disease. *Blood* **123**, 3818–3827 (2014).
16. E. J. Kunkel, J. L. Dunne, K. Ley, Leukocyte arrest during cytokine-dependent inflammation in vivo. *J. Immunol.* **164**, 3301–3308 (2000).
17. R. A. Clemens, J. Chong, D. Grimes, Y. Hu, C. A. Lowell, STIM1 and STIM2 cooperatively regulate mouse neutrophil store-operated calcium entry and cytokine production. *Blood* **130**, 1565–1577 (2017).
18. N. Demaurex, S. Saul, The role of STIM proteins in neutrophil functions. *J. Physiol.* **596**, 2699–2708 (2018).
19. N. Steinckwich, P. Myers, K. S. Janardhan, N. D. Flagler, D. King, J. G. Petranka, J. W. Putney, Role of the store-operated calcium entry protein, STIM1, in neutrophil chemotaxis and infiltration into a murine model of psoriasis-inflamed skin. *FASEB J.* **29**, 3003–3013 (2015).
20. O. Lindemann, C. Strodthoff, M. Horstmann, N. Nielsen, F. Jung, S. Schimmelpfennig, M. Heitzmann, A. Schwab, TRPC1 regulates fMLP-stimulated migration and chemotaxis of neutrophil granulocytes. *Biochim. Biophys. Acta* **1853**, 2122–2130 (2015).
21. T. F. Robertson, A. Huttenlocher, Real-time imaging of inflammation and its resolution: It's apparent because it's transparent. *Immunol. Rev.* **306**, 258–270 (2022).
22. S. K. Yoo, Q. Deng, P. J. Cavnar, Y. I. Wu, K. M. Hahn, A. Huttenlocher, Differential regulation of protrusion and polarity by PI3K during neutrophil motility in live zebrafish. *Dev. Cell* **18**, 226–236 (2010).
23. R. W. Beerman, M. A. Matty, G. G. Au, L. L. Looger, K. R. Choudhury, P. J. Keller, D. M. Tobin, Direct in vivo manipulation and imaging of calcium transients in neutrophils identify a critical role for leading-edge calcium flux. *Cell Rep.* **13**, 2107–2117 (2015).
24. A. Bohineust, Z. Garcia, B. Corre, F. Lemaitre, P. Bousso, Optogenetic manipulation of calcium signals in single T cells in vivo. *Nat. Commun.* **11**, 1143 (2020).
25. G. Ma, L. He, S. Liu, J. Xie, Z. Huang, J. Jing, Y. T. Lee, R. Wang, H. Luo, W. Han, Y. Huang, Y. Zhou, Optogenetic engineering to probe the molecular choreography of STIM1-mediated cell signaling. *Nat. Commun.* **11**, 1039 (2020).
26. E. A. Francis, V. Heinrich, Extension of chemotactic pseudopods by nonadherent human neutrophils does not require or cause calcium bursts. *Sci. Signal.* **11**, eaal4289 (2018).
27. N. Watanabe, J. Suzuki, Y. Kobayashi, Role of calcium in tumor necrosis Factor-α Production by activated macrophages. *J. Biochem.* **120**, 1190–1195 (1996).
28. A. Braun, J. E. Gessner, D. Varga-Szabo, S. N. Syed, S. Konrad, D. Stegner, T. Vogtle, R. E. Schmidt, B. Nieswandt, STIM1 is essential for Fcgamma receptor activation and autoimmune inflammation. *Blood* **113**, 1097–1104 (2009).
29. M. S. Schappe, K. Szteyn, M. E. Stremska, S. K. Mendu, T. K. Downs, P. V. Seegren, M. A. Mahoney, S. Dixit, J. K. Krupa, E. J. Stipes, J. S. Rogers, S. E. Adamson, N. Leitinger, B. N. Desai, Chanzyme TRPM7 mediates the Ca^{2+} influx essential for lipopolysaccharide-induced toll-like receptor 4 endocytosis and macrophage activation. *Immunity* **48**, 59–74.e5 (2018).
30. M. Vaeth, I. Zee, A. R. Concepcion, M. Maus, P. Shaw, C. Portal-Celhay, A. Zahra, L. Kozhaya, C. Weidinger, J. Philips, D. Unutmaz, S. Feske, Ca^{2+} signaling but not store-operated Ca^{2+} entry is required for the function of macrophages and dendritic cells. *J. Immunol.* **195**, 1202–1217 (2015).
31. Q. Chen, Y. Zhou, L. Zhou, Z. Fu, C. Yang, L. Zhao, S. Li, Y. Chen, Y. Wu, Z. Ling, Y. Wang, J. Huang, J. Li, TRPC6-dependent Ca^{2+} signaling mediates airway inflammation in response to oxidative stress via ERK pathway. *Cell Death Dis.* **11**, 170 (2020).
32. Z. Su, P. Zhang, Y. Yu, H. Lu, Y. Liu, P. Ni, X. Su, D. Wang, Y. Liu, J. Wang, H. Shen, W. Xu, H. Xu, HMGB1 facilitated macrophage reprogramming towards a proinflammatory M1-like phenotype in experimental autoimmune myocarditis development. *Sci. Rep.* **6**, 21884 (2016).
33. F. Barros-Becker, P. Y. Lam, R. Fisher, A. Huttenlocher, Live imaging reveals distinct modes of neutrophil and macrophage migration within interstitial tissues. *J. Cell Sci.* **130**, 3801–3808 (2017).
34. M. Nguyen-Chi, B. Laplace-Builhe, J. Travnickova, P. Luz-Crawford, G. Tejedor, Q. T. Phan, I. Duroux-Richard, J. P. Levraud, K. Kissa, G. Lutfalla, C. Jorgensen, F. Djouad, Identification of polarized macrophage subsets in zebrafish. *eLife* **4**, e07288 (2015).
35. K. Westphalen, G. A. Gusarova, M. N. Islam, M. Subramanian, T. S. Cohen, A. S. Prince, J. Bhattacharya, Sessile alveolar macrophages communicate with alveolar epithelium to modulate immunity. *Nature* **506**, 503–506 (2014).
36. J. M. Gee, N. A. Smith, F. R. Fernandez, M. N. Economo, D. Brunert, M. Rothermel, S. C. Morris, A. Talbot, S. Palumbos, J. M. Ichida, J. D. Shepherd, P. J. West, M. Wachowiak, M. R. Capecchi, K. S. Wilcox, J. A. White, P. Tvrdik, Imaging activity in neurons and glia with a Polr2a-based and cre-dependent GCaMP5G-IRES-tdTomato reporter mouse. *Neuron* **83**, 1058–1072 (2014).
37. W. Weninger, M. Biro, R. Jain, Leukocyte migration in the interstitial space of non-lymphoid organs. *Nat. Rev. Immunol.* **14**, 232–246 (2014).
38. E. Smedler, P. Uhlen, Frequency decoding of calcium oscillations. *Biochim. Biophys. Acta* **1840**, 964–969 (2014).
39. X. Zhou, Z. Li, Z. Wang, E. Chen, J. Wang, F. Chen, O. Jones, T. Tan, S. Chen, H. Takeshima, J. Bryant, J. Ma, X. Xu, Syncytium calcium signaling and macrophage function in the heart. *Cell Biosci.* **8**, 24 (2018).
40. K. Thurley, S. C. Tovey, G. Moenke, V. L. Prince, A. Meena, A. P. Thomas, A. Skupin, C. W. Taylor, M. Falcke, Reliable encoding of stimulus intensities within random sequences of intracellular Ca^{2+} spikes. *Sci. Signal.* **7**, ra59 (2014).
41. D. W. Goldman, F. H. Chang, L. A. Gifford, E. J. Goetzl, H. R. Bourne, Pertussis toxin inhibition of chemotactic factor-induced calcium mobilization and function in human polymorphonuclear leukocytes. *J. Exp. Med.* **162**, 145–156 (1985).
42. G. J. Spangrude, F. Sacchi, H. R. Hill, D. E. Van Epps, R. A. Daynes, Inhibition of lymphocyte and neutrophil chemotaxis by pertussis toxin. *J. Immunol.* **135**, 4135–4143 (1985).
43. N. Dixit, M. H. Kim, J. Rossaint, I. Yamayoshi, A. Zarbock, S. I. Simon, Leukocyte function antigen-1, kindlin-3, and calcium flux orchestrate neutrophil recruitment during inflammation. *J. Immunol.* **189**, 5954–5964 (2012).
44. K. Ley, C. Laudanna, M. I. Cybulsky, S. Nourshargh, Getting to the site of inflammation: The leukocyte adhesion cascade updated. *Nat. Rev. Immunol.* **7**, 678–689 (2007).
45. S. Nourshargh, P. L. Hordijk, M. Sixt, Breaching multiple barriers: Leukocyte motility through venular walls and the interstitium. *Nat. Rev. Mol. Cell Biol.* **11**, 366–378 (2010).

Downloaded from https://www.science.org at University Montpellier on September 11, 2023

46. G. A. Brito, J. L. Falcao, S. N. Saraiva, A. A. Lima, C. A. Flores, R. A. Ribeiro, Histopathological analysis of rat mesentery as a method for evaluating neutrophil migration: Differential effects of dexamethasone and pertussis toxin. *Braz. J. Med. Biol. Res.* **31**, 1319–1327 (1998).
47. D. Grimes, R. Johnson, M. Pashos, C. Cummings, C. Kang, G. R. Sampedro, E. Tycksen, H. J. McBride, R. Sah, C. A. Lowell, R. A. Clemens, ORAI1 and ORAI2 modulate murine neutrophil calcium signaling, cellular activation, and host defense. *Proc. Natl. Acad. Sci. U.S.A.* **117**, 24403–24414 (2020).
48. V. A. Morikis, E. Masadeh, S. I. Simon, Tensile force transmitted through LFA-1 bonds mechanoregulate neutrophil inflammatory response. *J. Leukoc. Biol.* **108**, 1815–1828 (2020).
49. T. W. Chen, T. J. Wardill, Y. Sun, S. R. Pulver, S. L. Renninger, A. Baohan, E. R. Schreiter, R. A. Kerr, M. B. Orger, V. Jayaraman, L. L. Looger, K. Svoboda, D. S. Kim, Ultrasensitive fluorescent proteins for imaging neuronal activity. *Nature* **499**, 295–300 (2013).
50. H. Dana, Y. Sun, B. Mohar, B. K. Hulse, A. M. Kerlin, J. P. Hasseman, G. Tsegaye, A. Tsang, A. Wong, R. Patel, J. J. Macklin, Y. Chen, A. Konnerth, V. Jayaraman, L. L. Looger, E. R. Schreiter, K. Svoboda, D. S. Kim, High-performance calcium sensors for imaging activity in neuronal populations and microcompartments. *Nat. Methods* **16**, 649–657 (2019).
51. S. Feske, Calcium signalling in lymphocyte activation and disease. *Nat. Rev. Immunol.* **7**, 690–702 (2007).
52. N. Faust, F. Varas, L. M. Kelly, S. Heck, T. Graf, Insertion of enhanced green fluorescent protein into the lysozyme gene creates mice with green fluorescent granulocytes and macrophages. *Blood* **96**, 719–726 (2000).
53. S. Jung, J. Aliberti, P. Graemmel, M. J. Sunshine, G. W. Kreutzberg, A. Sher, D. R. Littman, Analysis of fractalkine receptor CX(3)CR1 function by targeted deletion and green fluorescent protein reporter gene insertion. *Mol. Cell. Biol.* **20**, 4106–4114 (2000).
54. S. Baez, An open cremaster muscle preparation for the study of blood vessels by in vivo microscopy. *Microvasc. Res.* **5**, 384–394 (1973).
55. M. Salvermoser, R. Pick, L. T. Weckbach, A. Zehrer, P. Lohr, M. Drechsler, M. Sperandio, O. Soehnlein, B. Walzog, Myosin 1f is specifically required for neutrophil migration in 3D environments during acute inflammation. *Blood* **131**, 1887–1898 (2018).
56. A. R. Kurz, M. Pruenster, I. Rohwedder, M. Ramadass, K. Schafer, U. Harrison, G. Gouveia, C. Nussbaum, R. Immler, J. R. Wiessner, A. Margraf, D. S. Lim, B. Walzog, S. Dietzel, M. Moser, C. Klein, D. Vestweber, R. Haas, S. D. Catz, M. Sperandio, MST1-dependent vesicle trafficking regulates neutrophil transmigration through the vascular basement membrane. *J. Clin. Invest.* **126**, 4125–4139 (2016).
57. A. Zehrer, R. Pick, M. Salvermoser, A. Boda, M. Miller, K. Stark, L. T. Weckbach, B. Walzog, D. Begandt, A fundamental role of Myh9 for neutrophil migration in innate immunity. *J. Immunol.* **201**, 1748–1764 (2018).
58. P. Uhlén, Spectral analysis of calcium oscillations. *Sci. STKE* **2004**, pl15 (2004).

Acknowledgments: We thank J. Truong for performing the chemotaxis microscopy experiments. **Funding:** This study was supported by the Deutsche Forschungsgemeinschaft through the collaborative research center 914 project B02 (to K.S. and S.M.), project B03 (to C.A.R.), project A10 (to C.S.), project Z03 (to B.W. and M.S.), and project Z01 (to S.M.); the collaborative research center 1123 project B07 (to K.S. and S.M.); the LMUexcellent (to K.S.); the DFG Clinician Scientist Programme PRIME (413635475 to K.P.); the Deutsche Zentrum für Herz-Kreislauf-Forschung (to K.S., C.S., and S.M.). The work was also supported by the European Research Council ERC-Starting grant "T-MEMORE" (ERC grant 947611) (to K.S.).
Author contributions: K.S. and F.T.M. conceived and designed the experiments. F.T.M., M.M., B.U., C.A.R., R.P., A.B., M.N., M.S., B.W., and K.S. performed and analyzed the intravital microscopy or cell migration assays. K.P. and F.T.M. performed isolation of peritoneal macrophages and in vitro microscopy. S.M. provided funding. C.S. provided mice. F.T.M. and K.S. analyzed the data and wrote the manuscript, which was reviewed by all of the authors.
Competing interests: The authors declare that they have no competing interests. **Data and materials availability:** All data needed to evaluate the conclusions in the paper are present in the paper or the Supplementary Materials.

Submitted 9 September 2020
Resubmitted 16 November 2021
Accepted 7 July 2022
Published 26 July 2022
10.1126/scisignal.abe6909

Downloaded from https://www.science.org at University Montpellier on September 11, 2023

Science Signaling

Intravital calcium imaging in myeloid leukocytes identifies calcium frequency spectra as indicators of functional states

Fitsumbirhan T. Mehari, Meike Miller, Robert Pick, Almke Bader, Kami Pekayvaz, Matteo Napoli, Bernd Uhl, Christoph A. Reichel, Markus Sperandio, Barbara Walzog, Christian Schulz, Steffen Massberg, and Konstantin Stark

Sci. Signal., **15** (744), eabe6909.
DOI: 10.1126/scisignal.abe6909

Decoding Ca2+ signals

The immune responses to infection and sterile inflammation are complex, involving the coordinated recruitment and activation of multiple cell types. To better understand the activation states of immune cells in the context of inflammation, Mehari *et al.* used various in vivo imaging techniques with transgenic Ca2+ reporter mice to measure the intensity and frequency of intracellular Ca2+ signals in macrophages and neutrophils as they responded to a laser-induced tissue injury. Analysis of these data revealed the kinetics of recruitment of tissue-resident macrophages and identified distinct patterns of intracellular Ca2+ signals in neutrophils that characterized the different stages of their recruitment from the blood to sites of injury. These findings suggest that in vivo monitoring of Ca2+ signals provides insights into the functional states of immune cells.

View the article online
https://www.science.org/doi/10.1126/scisignal.abe6909
Permissions
https://www.science.org/help/reprints-and-permissions

Downloaded from https://www.science.org at University Montpellier on September 11, 2023

Use of this article is subject to the Terms of service

Science Signaling (ISSN) is published by the American Association for the Advancement of Science. 1200 New York Avenue NW, Washington, DC 20005. The title *Science Signaling* is a registered trademark of AAAS.
Copyright © 2022 The Authors, some rights reserved; exclusive licensee American Association for the Advancement of Science. No claim to original U.S. Government Works